Transactions on Biomedicine and Health vol 1, © 1993 WIT Press, www.witpress.com, ISSN 1743-3525

The forward problem of electrocardiology incorporating detailed heart anatomy

P.R. Johnston & D. Kilpatrick
Department of Medicine, University of Tasmania, 43 Collins St., Hobart, Tasmania 7000, Australia

ABSTRACT

The forward problem of Electrocardiology is the determination of the body surface potential distribution given a specified potential distribution on the surface of the heart. The governing equation for the electric potential distribution inside a realistic torso containing the internal heart chambers is solved using the boundary element method (employing techniques using discontinuous elements).

The aim of developing this model is to gain an understanding of current flow within the thorax due to various conditions affecting the heart and to correlate these conditions with observed changes in the body surface electrocardiogram.

INTRODUCTION

The electrocardiogram is an essential tool in medical practice. It reflects the body surface potential distribution due to the electrical activity of the heart. To correlate these measured distributions with the pathological processes in the heart a detailed model of the thorax has been developed (including the great vessels and ventricular cavities). The model will be used to derive the body surface potentials for various cardiac sources. Recent work has suggested the necessity of including the great vessels in such computational models.

THE BODY MODEL

The computational domain is an inhomogeneous isotropic human thorax, consisting of heart, lungs, spine, sternum and general body tissue. Further, the heart is divided into regions of heart muscle and blood (the left and right atria and ventricles, the aorta and pulmonary artery). All regions

in the domain are assigned differing but constant resistivities and these are as follows (Rush et al., [1]): body tissue, 460 Ωcm; lungs, 2100 Ωcm, and blood 160 Ωcm. The heart muscle is not included in the computation domain (as the boundary conditions are applied on the surface of the heart muscle) and so no resistivity value is required. Also, bone is assumed to be totally non–conducting.

The geometry of the thorax is created from digitising a series of MRI scans from a human subject. On appropriate slices, the outlines of the thorax, heart, lungs, spine, sternum and heart vessels are recorded by computer. The points from a given surface are then extracted from each slice and concatenated together. Techniques of linear interpolation in a horizontal plane are then used to create a surface mesh consisting of an equal number of evenly spaced nodes in each horizontal layer of a given organ.

Digitisation and interpolation results in a set of surfaces representing the outer surface of the thorax, the spine, the sternum, the left and right lungs, the epicardium, the left and right ventricles, the left and right atria, the aorta and the pulmonary artery. Figure 1 is a cross–sectional view of the reconstructed thorax showing the body surface, lungs, spine, epicardium, left and right ventricles and the aorta (note the similarity to the usual MRI or CT scans). This torso model is an improvement over previous models (Gulrajani and Mailloux, [2]) in that there is an electrical pathway from the internal blood masses to the body surface. The three dimensional mesh, consisting of quadrilaterals, is suitable for the solution of the governing differential equations for electric potential using the boundary element method.

GOVERNING EQUATIONS

The electric potential, u, in an inhomogeneous isotropic thorax is governed by Laplace's equation

$$\nabla \cdot (\sigma \nabla u) = 0 \tag{1}$$

with no current flow through the body surface and a specified potential distribution on the surface of the heart,

$$\nabla u \cdot \mathbf{n} = 0 \quad \text{and} \quad u = h(x, y, z) \tag{2}$$

where $\mathbf{n}$ represents the normal vector to the surface and $\sigma(x, y, z)$ the conductivity, unique for each organ. Since the thorax is inhomogeneous, conditions of continuous potential and current flow are required on the internal surfaces of the body. That is,

$$u_1 = u_2 \quad \text{and} \quad \sigma_1 \nabla u_1 \cdot \mathbf{n} = -\sigma_2 \nabla u_2 \cdot \mathbf{n} \tag{3}$$

where the subscripts 1 and 2 refer to different sides of a given boundary.

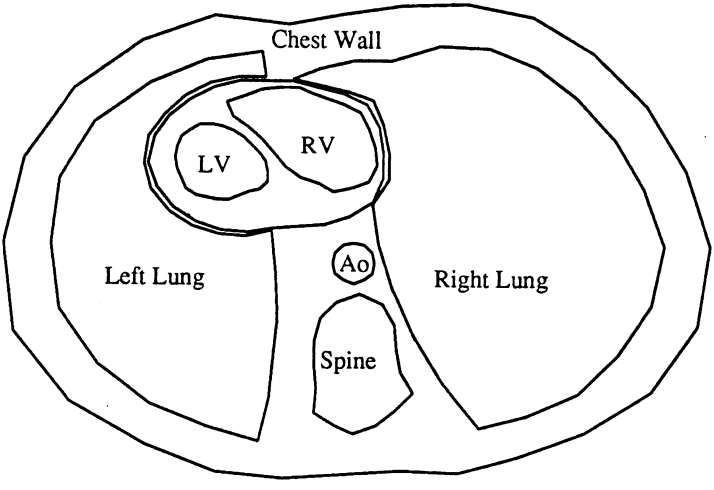


Figure 1: Cross Section of Reconstructed Body

Solving equation (1) subject to conditions (2) and (3) is referred to as the forward problem in electrocardiology (predicting body surface potentials from given heart surface potential distributions). This can be expressed in a matrix form as

$$\mathbf{Th} = \mathbf{b} \tag{4}$$

where $\mathbf{T}$ is the forward transfer matrix, $\mathbf{h}$ is a vector of heart surface potentials and $\mathbf{b}$ a vector of body surface potentials. Hence, given a distribution of potential on the surface of the heart, $\mathbf{h}$, it is possible, by matrix multiplication, to determine the body surface potential distribution, $\mathbf{b}$.

Due to the complex shape of the human body, numerical methods are required to solve the governing equations. Possible solution techniques are the finite difference method, the finite element method and the boundary element method. Here the boundary element method was chosen because creating a two dimensional mesh on the surfaces of the thorax is much simpler than creating a three dimensional mesh in the volume of the thorax. The cost in implementing this method is the loss of the sparse matrices which arise with the use of the other two methods mentioned, but, on the other hand, fewer nodes are required.

IMPLEMENTATION OF THE BOUNDARY ELEMENT METHOD

Since the human thorax is inhomogeneous, it must be divided into subregions where the conductivity is assumed constant. Therefore the governing equation for each region is

$$\nabla^2 u = 0 \tag{5}$$

with the conductivities introduced through the interface conditions.

To actually implement the boundary element method, the governing differential equation is converted into an integral equation using a weighted residuals approach. The residuals are minimised by orthogonalising them with respect to a weighting function, u^*, defined to be a fundamental solution of Laplace's equation (Brebbia and Dominguez, [3]). Lettting

$$q = \frac{\partial u}{\partial n} \tag{6}$$

means the fundamental equation for the boundary element method can be written as

$$c_i u_i + \int_\Gamma u q^* d\Gamma = \int_\Gamma q u^* d\Gamma. \tag{7}$$

Here the subscript i refers to an arbitrary node in the mesh, Γ is the boundary of the region under consideration and c_i is a coefficient to be determined.

For three–dimensional problems

$$u^* = \frac{1}{4\pi}\left(\frac{1}{r}\right) \tag{8}$$

where r is the distance from the point i to the surface Γ and $q^*(= \frac{\partial u^*}{\partial \mathbf{n}})$ is given by

$$q^* = -\frac{1}{4\pi}\frac{\mathbf{r}}{r^3}\frac{\partial r}{\partial \mathbf{n}}. \tag{9}$$

If the surface is discretised into N elements then equation (7) can be written as

$$c_i u_i + \sum_{j=1}^{N} \int_{\Gamma_j} u q^* d\Gamma = \sum_{j=1}^{N} \int_{\Gamma_j} q u^* d\Gamma. \tag{10}$$

In this paper, the surface is discretised into quadrilateral regions and there is a linear variation of potential from one node to all adjacent nodes. Other discretisations are possible (for example triangles) as well as other variations in potential between nodes. This choice of elements and variation together are described as linear quadrilateral elements. They represent a balance between continuity and accuracy of the solution and computation time.

Using these basis functions it is possible to evaluate the integrals in equation (10) in terms of the potentials $\mathbf{u}$ and potential gradients $\mathbf{q}$ at the surface nodes. Hence equation (10) can be written in a matrix form as

$$\mathbf{Hu} = \mathbf{Gq} \tag{11}$$

where the constants, c_i, are evaluated from $\mathbf{HI} = \mathbf{0}$ ($\mathbf{I}$ being a vector of 1's) (Brebbia and Dominguez, [3]).

A matrix equation of the form (11) is required for each subdomain (or organ) in the model, as well as for the left and right blood masses inside the heart. These separate matrix equations are related through the interface conditions (3) and, finally, application of the boundary conditions (2) and rearrangement results in the matrix equation (4).

The model of the thorax, reconstructed in the manner described previously, consists of over 4000 nodes and 4000 linear quadrilateral elements. Nearly half of the nodes and elements are on the surfaces of the heart and its chambers due to the complicated shape of the internal vessels. In fact, it became necessary to partition, with interfaces, the left side vessels into the left ventricle and the left atrium and divide the aorta into two parts, one leading from the left ventricle to the epicardial surface and the second from the epicardial surface to the end of the aorta. These partitions and the interfaces define more convex shapes, leading to more accurate numerical results. Similar partitions and interfaces are created for the right side vessels.

Another important aspect of the numerical approach to this problem is the use of discontinuous elements (Brebbia and Dominguez, [3]). These are required at all intersections in the model, that is, around the interfaces described above, and on the top surface of the heart at the exit of the pulmonary artery and aorta. At the points of surface intersection several normals exist, each having different directions, contradicting the assumptions of the boundary element method. To overcome this, the nodes are "withdrawn" into the elements along one of the sides, creating discontinuous elements. This has the effect of increasing the number of nodes (but not the number of elements), and giving each node a unique normal. Each node is moved in a distance of 0.1 times the length of its appropriate side. Numerical integration is still performed over the full size element by extrapolating the element back to to its full size and defining a new set of basis functions.

NUMERICAL SIMULATIONS

One aim of developing such a detailed model is to study the effects of subendocardial ischaemia on the resulting body surface maps. It has been suggested that current paths for subendocardial ischaemia pass through the low resistance pathway provided by the intracavity blood, out of the great vessels and back onto the epicardium (Kilpatrick et al., [4]). This would result in the top surface of the heart appearing electrically positive, relative to the remainder of the epicardium. Further, the subsequent body surface maps should be similar to that produced by ischaemia solely on the top of the heart (i.e. a superior infarction).

A forward transfer matrix, $\mathbf{T}$, is constructed using the methods outlined

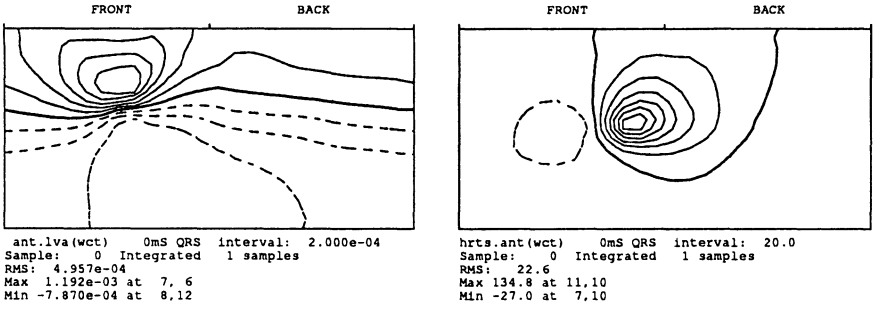


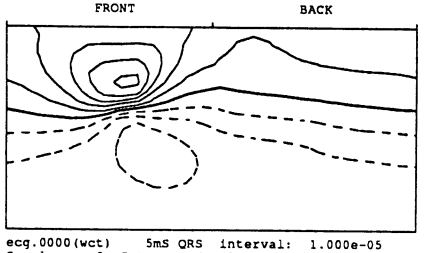
Figure 2: Body Surface Maps for Endocardial and Epicardial Ischaemic Regions

above. The matrix relates potentials on the epicardial surface and the left and right ventricle and atria surfaces to body surface potentials. Ischaemia is simulated in a non-dimensional fashion by defining regions of normal heart muscle to have zero potential on their surfaces and ischaemic muscle to have a potential value of 1.0. These values are combined into a vector, h, and the resulting body surface potential distribution, b, calculated by matrix multiplication as defined by equation (4).

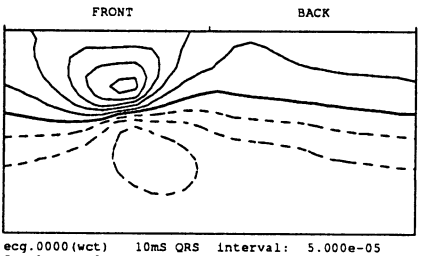
The first simulation considered is that of a comparison of endocardial to epicardial ischaemia. Ischaemia was created on the left anterior wall of the left ventricle (endocardial) and on the heart surface nearest to this endocardial region. The results of the simulations are displayed in Figure 2 as body surface maps. Each map has been translated relative to a Wilson Central Terminal, where the average of the potentials at the left and right shoulders and the left waist is subtracted from each potential value. This has the effect of creating a zero line in each map, even though the initial potentials are either zero or one.

Inspection of the maps shows that they are distinctly different in shape with their respective zero lines, the thick solid line between the dotted (negative potential) lines and the thin solid (positive potential) lines, following totally different paths. It appears, given the positions of the respective maxima and minima, that the maps have been rotated through approximately ninety degrees.

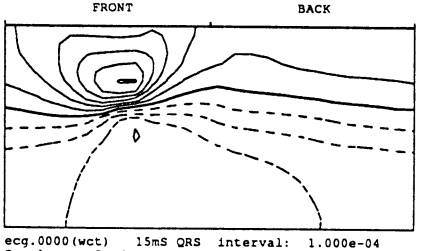
Another application of this technique is to examine the results of depolarisation sequences. As a second simulation, body surface maps for the first 35 msec of the QRS are calculated where the source is approximated from data recorded in the isolated human heart (Durrer et al., [5]). Wave front propagation is achieved by assigning nodes in front of the wave a potential of zero and those behind it a value of one. The resulting body surface maps are shown in Figure 3. Epicardial breakthrough is shown after 31 msecs and is



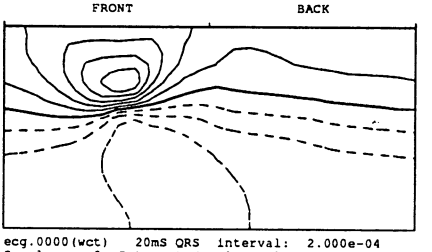
ecg.0000(wct) 5mS QRS interval: 1.000e-05
Sample: 0 Integrated 1 samples
RMS: 2.203e-05
Max 5.251e-05 at 7, 6
Min -3.508e-05 at 8,12



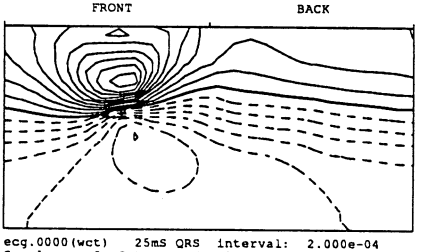
ecg.0000(wct) 10mS QRS interval: 5.000e-05
Sample: 0 Integrated 1 samples
RMS: 1.106e-04
Max 2.639e-04 at 7, 6
Min -1.759e-04 at 8,12



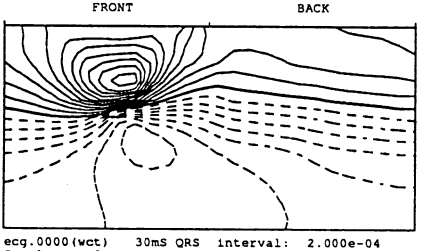
ecg.0000(wct) 15mS QRS interval: 1.000e-04
Sample: 0 Integrated 1 samples
RMS: 2.550e-04
Max 6.087e-04 at 7, 6
Min -4.057e-04 at 8,12



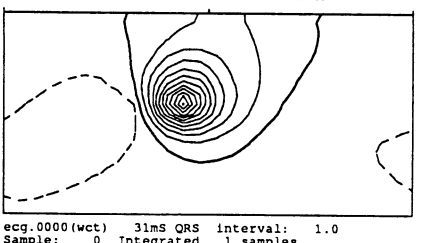
ecg.0000(wct) 20mS QRS interval: 2.000e-04
Sample: 0 Integrated 1 samples
RMS: 4.710e-04
Max 1.122e-03 at 7, 6
Min -7.501e-04 at 8,12



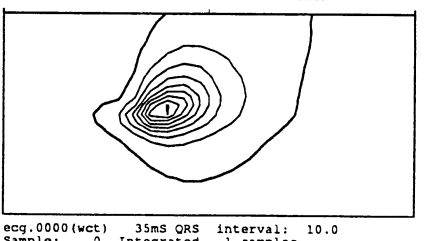
ecg.0000(wct) 25mS QRS interval: 2.000e-04
Sample: 0 Integrated 1 samples
RMS: 8.855e-04
Max 2.105e-03 at 7, 6
Min -1.411e-03 at 8,12



ecg.0000(wct) 30mS QRS interval: 2.000e-04
Sample: 0 Integrated 1 samples
RMS: 9.702e-04
Max 2.307e-03 at 7, 6
Min -1.546e-03 at 8,12



ecg.0000(wct) 31mS QRS interval: 1.0
Sample: 0 Integrated 1 samples
RMS: 1.5
Max 11.2 at 11,10
Min -1.6 at 7,11



ecg.0000(wct) 35mS QRS interval: 10.0
Sample: 0 Integrated 1 samples
RMS: 11.4
Max 81.2 at 10,10
Min -6.0 at 6, 7

Figure 3: Body Surface Maps for the First 35 msecs of QRS

simulated by one node on the heart surface being assigned a potential value of one, with the remainder having a potential value of zero. Note the distinct difference between pre- and post epicardial breakthrough body surface maps. Also worth noting is the large increase in potential values observed after epicardial breakthrough. This indicates the small contribution of the initial endocardial depolarisation compared to the epicardial breakthrough.

CONCLUSIONS

This paper has presented an implementation of the boundary element method (exploiting discontinuous elements) to solve the governing equation for electric potential in a realistic human thorax containing detailed anatomy of the heart. Each surface in the model was reconstructed from a series of MRI scans and represented in three dimensions as sets of quadrilateral surfaces.

The model has been used to investigate body surface maps resulting from endocardial ischaemia in the left ventricle. When compared to epicardial ischaemia in the same region, the body surface maps were considerably different. Also, the magnitudes of the body surface potentials resulting from epicardial ischaemia are much greater than those of endocardial ischaemia.

The model has also been used to study the early QRS body surface maps. When epicardial breakthrough occurs there is a significant change in the appearance of the body surface map.

REFERENCES

[1] Rush, S., Abildskov, J. A., and McFee, R. Resistivity of body tissues at low frequencies. *Circulation Research*, Vol. 12, pp. 40–50, 1963.

[2] Gulrajani, R. M. and Mailloux, G. E. A simulation study of the effects of torso inhomogeneities on electrocardiographic potentials, using heart and torso models. *Circ. Res.*, Vol. 52, pp. 45–56, 1983.

[3] Brebbia, C. A. and Dominguez, J. *Boundary Elements An Introductory Course*. Computational Mechanics Publications, Southampton, second edition, 1992.

[4] Kilpatrick, D., Walker, S. J., and Bell, A. J. The importance of the great vessels in the genesis of the electrocardiogram. *Circulation Research*, Vol. 66, pp. 1081–1088, April 1990.

[5] Durrer, D., van Dam, R., Freud, G. E., Janse, M. J., Meijler, F. L., and Arzbaecher, R. C. Total excitation of the isolated human heart. *Circulation*, Vol. 41, pp. 899–912, 1970.